Dynamic response of a novel flexible wave energy converter under regular waves

X.Li, Q. Xiao, Y.Luo, G.Moretti, M.Fontana, M.Righi

Abstract—**Different from the traditional rigid body WECs, a flexible WEC consisting of flexible material is numerically modeled in this paper. A fully coupled fluid-structure interaction solver that can cope with the dynamic interplay between the flexible membrane and the surrounding fluid is developed. The fluid field is resolved by computational fluid dynamics (CFD) method, where a multi-phase flow solver is chosen to simulate oceanic waves. The flexible body is modeled as a two-dimensional beam. The data exchange between the two solvers is achieved by a coupling strategy. With this tool, the various flexible deformations can be captured with the wave propagating. The detailed flow field is obtained in the vicinity of the membrane along with the dynamic force acting on it. Although a linear structure model is used, the CFD results qualitatively repeat the experiment data. Our results show that the incident wave period influences the membrane deformation. In addition, adding a collector at the top of the membrane can increase the extent of deformation attributed to the increased wave excitation force.**

Keywords— **flexible WEC, CFD, Multi-body Dynamic, Fluid-Structure Interaction**

I. Introduction

With the development of industry, the environmental problem is getting more and more serious. Wave energy, as one representative of clean energy, has been studied for a few decades. Many representative prototypes of wave energy converters (WECs) were invented and developed up to the full-scale, e.g., Pelamis Wave Power [1] and Aquamarine Power Oyster [2]. However, no WECs have been applied on a large scale commercially so far. One common problem of WECs is their adaptability to different wave conditions. Most devices can only produce considerable power with a specific condition, e.g., a certain range of wave frequencies. Their performance decreases sharply out of the preferred wave range. This hinders WECs usage under a variety of wave conditions. Another problem is that the cost is still too high for the manufacturing and matainance of WECs, compared to their profits.

To overcome these drawbacks, rubber-like polymeric materials are getting more and more attention, as they can be used to design a special class of power take-off (PTO) systems for WECs, the so called dielectric elastomer generators (DEGs) [3]. Dielectric elastomer (DE) materials, such as rubber or silicone, are inexpensive and highly adaptable to extreme sea conditions. Moretti et.al. [4] applied DE materials into a traditional oscillating water column (OWC). A detailed study was carried out experimentally, providing a promising demonstration of the operation and effectiveness of OWCs based on DEGs. Wave tank tests were carried out, in which a notable maximum fraction of 18% of the input wave energy was converted into electricity. In conjunction with the above work, an oscillating wave surge energy converter was proposed and studied using a simplified hydrodynamic model with the aim of identifying an optimal control strategy for maximising the power production [5]. The results shows that the estimated power outputs can be as large as around 1.5 MW with 1.5 m^3 elastomeric material.

There is little research on flexible WECs, especially studies using numerical analysis tool . Among them, either a non-coupled method, or a simplified model based on linear potential flow theory is widely used. With such linear potential flow theory, Michailides studied the response of a flexible structure made up of 4 rigid plates, connected by constraints [6]. This flexible structure works as a breakwater, as well as a generator. The results obtained a desired level for both wave energy production

X. Li is with Department of Naval Architecture, Ocean and Marine Engineering, University of Strathclyde, UK (e-mail: xiang.li@strath.ac.uk).

Q. Xiao is with Department of Naval Architecture, Ocean and Marine Engineering, University of Strathclyde, UK (e-mail: qing.xiao@strath.ac.uk) (corresponding author).

Y . Luo is with Department of Naval Architecture, Ocean and Marine Engineering, University of Strathclyde, UK (e-mail: y.luo@strath.ac.uk).

G. Moretti is with TeCIP Institute, Scuola Superiore Sant'Anna, Italy (giacomo.moretti@santannapisa.it).

M.Fontana is with Department of Industrial Engineering, University of Trento, Italy (marco.fontana-2@unitn.it).

M. Righi is with TeCIP Institute, Scuola Superiore Sant'Anna, Italy (righi.michele23@gmail.com).

and protection effectiveness. Zhang et al. studied the effects of structural flexibility on the maximum wave energy conversion by two interconnected floaters [7]. The coupled effects of structural deformation and hydrodynamic interaction were considered using an approximate approach based on the discrete-modules and Euler-Bernoulli beam bending. It was found that for a relatively small wavelength, the structural flexibility enhances the power capture. Babarit et.al. studied a bulge-wave WEC made using dielectric elastomer material. Lumped parameter modelling was used based on spectral decomposition, and potential flow theory [8]. Also with potential flow theory, boundary element mothod (BEM) was combined to study a WEC based on a rubber bag submerged under water [9] . With a distributed-parameter analytical approach, Renzi coupled the linear piezoelectric constitutive equations with the potential-flow equations to cope with the surface water waves. A submerged piezoceramic plate WEC is studied [10] . Zheng et al. studied the performance of a circular plate under regular waves. The effect of the radius and edge condition is investigated [11]. It can be seen that less attention has been paid to the coupled fluid-structure interaction (FSI) effect of a flexible WEC. The details of fluid flow were ignored in the previous studies, e.g., viscous, vortex and nonlinear effects. These aspects play a important part in a flexible WEC response, especially when the deformation is sensitive to the surrounding fluid field. This paper aims to investigate a flexible-membrane WEC, in which the power generation is directly related to the deformation of a functional DE membrane generated by the fluid force difference applied on the membrane, proposed by Moretti et.al. [3]. To solve this problem, a high fidelity computational fluid dynamics (CFD) method together with a structure analysis method is used with a strong coupling strategy, with which the coupled fluid-structure interaction can be fully observed. As the first step to numerical analyze such complex non-linear FSI system, some simplifications are made in this study. For example, the problem is consider as two-dimensional while the experiment device is three-dimensional. In addition, the deformation of DE material is represented by a beam model instead of a membrance.

II. NUMERICAL MODEL

For the flexible WEC, a strong fluid-structure interaction exists, thus a fully coupled FSI tool is developed to solve such problem. To be specific, the fluid problem is solved by a transient numerical solver while the flexible structure response is calculated by Multibody Dynamics. To exchange data between the two solvers at each iteration, an adapter code is developed [12].

The CFD solver is developed based on the multi-phase solver interFOAM provided in OpenFOAM [13]. The governing equation of this is the continuity equation and incompressible Navier-Stokes equations:

$$\nabla \cdot \boldsymbol{U} = 0 \tag{1}$$

$$\begin{aligned} P\frac{\partial \rho \boldsymbol{U}}{\partial t} + \nabla \cdot \left(\rho \left(\boldsymbol{U} - \boldsymbol{U}_g \right) U \right) = -\nabla P_d - \boldsymbol{g} \cdot \boldsymbol{x} \nabla \rho \\ + \nabla \left(\mu_{eff} \nabla \boldsymbol{U} \right) + \left(\nabla \boldsymbol{U} \right) \cdot \mu_{eff} + \boldsymbol{f}_\sigma \end{aligned} \tag{2}$$

where $\boldsymbol{U}$ is the velocity of the fluid and ρ is the density. $\boldsymbol{U}_g$ denotes the speed of the motion of the mesh grid, which is zero for a fixed boundary. P_d denotes the dynamic pressure. $\boldsymbol{g}$ is the gravity acceleration. μ_{eff} denotes the effective dynamic viscosity, $\boldsymbol{f}_\sigma$ is the surface tension which is only considered on the free surface. The Volume of Fluid (VOF) method is used to capture the free surface.

$$\frac{\partial \alpha}{\partial t} + \nabla \cdot \left(\left(\boldsymbol{U} - \boldsymbol{U}_g \right) \alpha \right) + \nabla \cdot \left(\boldsymbol{U}_r \left(1 - \alpha \right) \alpha \right) = 0 \tag{3}$$

where α is the phase fraction denoting the form of the fluid. α=1 means the fluid is water and α=0 means air. U_r is is an artificial velocity field used to compress the interface between water and air, which is determined by the maximum magnitude of the velocity near the free surface. Fluid densityρ and viscosity μ can also be described by phase fraction:

$$\rho = \alpha \rho_w + \left(1 - \alpha \right) \rho_\alpha \tag{4}$$

$$\mu = \alpha \mu_w + \left(1 - \alpha \right) \mu_\alpha \tag{5}$$

where subscripts w and a denote the liquid and gas, respectively. To generate waves, the velocity is prescribed at the inlet boundary based on Stokes second-order wave theory. The vertical velocity u and horizontal velocity w is described by:

$$\begin{aligned} u = \frac{\pi H}{T} \frac{\cosh k\left(z + d \right)}{\sinh kd} \cos\theta \\ + \frac{3\pi H}{4T} \left(\frac{\pi H}{L} \right) \frac{\cosh 2k\left(z + d \right)}{\sinh^4 kd} \cos 2\theta \end{aligned} \tag{6}$$

$$\begin{aligned} w = \frac{\pi H}{T} \frac{\sinh k\left(z + d \right)}{\sinh kd} \sin\theta \\ + \frac{3\pi H}{4T} \left(\frac{\pi H}{L} \right) \frac{\sinh 2k\left(z + d \right)}{\sinh^4 kd} \sin 2\theta \end{aligned} \tag{7}$$

where H is the wave height, T is the wave period, k is the wave number, L is the wave length, d is the water depth. θ is the phase.

The motion and the internal force of the structure are solved by the multi-body dynamic solver MBDyn [14]. For each geometrical entity, the governing equations in MBDyn are the first-order Newton-Euler equation together with the constraint equations as follows,

$$\boldsymbol{M}\dot{\boldsymbol{x}} = \boldsymbol{p} \tag{8}$$

$$\dot{\boldsymbol{p}} + \boldsymbol{\phi}_x^T \boldsymbol{\lambda} = \boldsymbol{f}\left(\boldsymbol{x}, \dot{\boldsymbol{x}}, t\right) \tag{9}$$

$$\boldsymbol{\phi}\left(\boldsymbol{x}, t\right) = 0 \tag{10}$$

where M denotes the inertia matrix of the rigid body, x denotes the translational and rotational parameters in the global reference frame. p refers to the momentum of the body. λ denotes the vector of the Lagrange multipliers for the constraints; f is the external force and moment vector exerted upon the body which might be related to its displacement and velocity as well as time. ϕ is a set of kinematic constraints applied on the body and ϕ_x^T is the Jacobian of ϕ with respect to the generalized coordinates.

The data exchange between the two solvers is transferred by an interface. The CFD solver and the structural solver run simultaneously in separate computer processes and they exchange the data with the help of TCP/IP protocol. The structural force that is calculated in the CFD solver is transformed into the structural solver. By using the force data, it predicts the response of the WEC model and transfers the motion data to CFD solver. The CFD mesh is then updated, followed up by an update of the entire flow field. The communication between the two solvers is completed at each iteration in each time step so that fully coupling is achieved with a robust and fast convergence.

This coupled tool has been validated for strong FSI problems, showed its good reliability in other studies [10]. Moreover, the accuracy of numerical wave generating is verified in our previous studies [15], thus these are not reiterated in this paper.

III. MODEL DESCRIPTION

The flexible WEC studied in this paper is based on the experiment conducted by Righi et.al. [16] The model is simplified as a 2D model aming to reduce computational cost, as shown in Figure 1. The origin of coordinates is located on the static water level (SWL). x points to the wave direction and z is opposite to the gravity direction. The whole device is submerged underwater where the membrane in the middle is the key part to extract power from waves. A collector above it can hold part of the water mass above, aiming to increase the hydrodynamic force. Below the membrane, there is an air chamber. The air pressure inside the chamber is assumed to be the same as the atmospheric pressure, which is a simplified model. In the actual device, the pressure varies as a function of the membrane deformation.

When wave comes over, the pressure difference between the up and lower surfaces of membrance causes it to deform continuously like a balloon. In this process, the membrane is stretched, thus leading to a change of the thickness. The DE membrane holds stretchable electrodes on both faces and functions as a variable capacitor. Deformations induced by the hydrodynamic pressure cause a variation in the membrane surface and thickness, hence leading to variations in the DEG capacitance. By properly modulating the voltage applied on the DEG as a function of the current deformation (e.g., allowing a charge on the DEG during the phases in which its capacitance decreases, and keeping it uncharged while its capacitance is increasing) allows converting part of the input mechanical energy into electrical energy [16]. With a simplified model in this paper, we mainly study the motion responses of the membrane while the effect of voltage and the power take-off model is not applied.

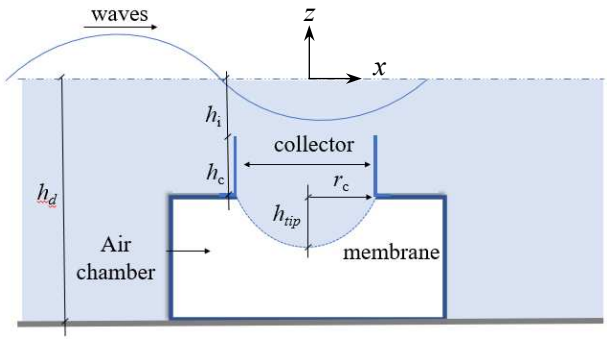

Figure 1 Sketch of a flexible WEC model

In our numerical simulation, the parameters for the geometry are the same as those in the experiment [16], in which the model is a scaled version of the considered WEC with a scale factor of 1:30/1:40. The wave parameters are also scaled based on this criteria. The distance between the top of the collector and the SWL h_i is 0.1 m, the height h_c and the radius r_c of the collector (which is half of the collector's length in this problem) is 0.08 m and 0.065 m respectively. The unstretched length of the membrane is equal to the diameter of the collector. The tip displacement of the membrane h_{tip} changes with time, denoting the degree of the deformation, which is also an indicator of the generated power. The whole WEC device is fixed on the seabed and the water depth h_d is 1.114 m.

The Stokes second-order waves are generated with a wave height of 0.1 m, and the wave period ranges from 0.8 s to 2.0 s. The unscaled waves period ranges from 5 s to 12 s, which is consistent with the real sea state for WEC operation.

The deformation of the membrane relies deeply on the material properties. In the experiment, a hyper-elastic rubber is utilized with nonlinear stiffness. At the beginning under the static pressure condition, the stiffness is large enough to avoid large initial deformation Δh_1.

Afterwards, when the dynamic pressure appears which is caused by wave, with the increase of strain, the stiffness becomes much smaller, leading to a large deformation Δh_2. For such a flexible WEC device, the dynamic deformation Δh_2 contributes most to the power generation. The membrane is designed in a way that it exhibits a relatively low stiffness in the neighborhood of its equilibrium configuration, hence potentially undergoing large deformations. In our numerical model, we use a linear elastic material model, where the the stress-strain relationship is linear, to simulate the dynamic response of the membrane. The Young's Modulus used is $2.5e^6$ Pa with a Poisson's ratio of 0.35. The linear model is different from the hyper-elastic material used in the experiment. This makes it easier to isolate some basic phenomena with less interference factors. Because the static pressure is much larger than the dynamic pressure, Δh_2 can be much smaller than Δh_1, as shown in Figure 2. There is no pre-strain in this model.

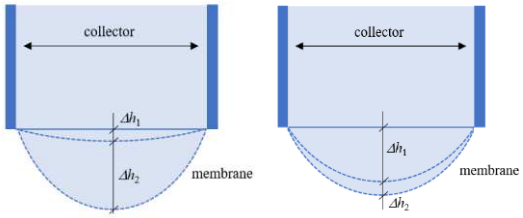

Figure 2 Deformation under static pressure with (a) hyper-elastic model (b) linear-elastic model

Even with such simplified model, we are able to replicate qualititave trends of experimental testing under different regular waves, such as the membrane deformations. In addition, with a coupled CFD simulation, the fluid field around the structure can be fuly resolved and analysed, which is not an easy task in the experiment.

The CFD mesh is presented in Figure 3. The total number of the cell of present mesh is 75000. As shown in Figure 3 (a), the free surface is refined in the wave height direction to better capture the wave profile. The mesh is also refined around the membrane and the collector where the flow field may be complicated, as indicated in Figure 3 (b). The boundary condition of the membrane is a non-slip wall boundary for fluid velocity and zero gradient for pressure. The velocity and pressure at the inlet boundary are prescribed by the regular wave theory, and both are set to be zero gradient at the outlet boundary. As it is a 2D simulation, the boundary type of the front and back is set to empty, which means it does not solve in y-axis.

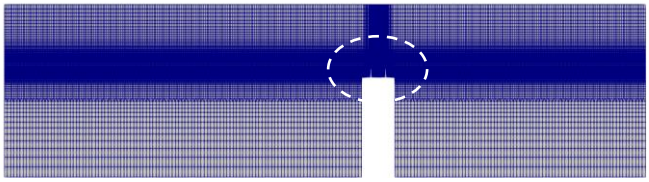

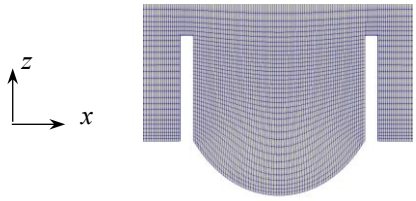

Figure 3 CFD mesh (a) of whole wave tank (b) around the membrane

The time step for all cases is 0.001s, which is less than 1/1000 of the wave period. To solve the pressure-velocity coupling for a transient simulation, PIMPLE (a combination of PISO and SIMPLE) algorithm is utilized. A second-order Crank-Nicolson scheme is used for temporal discretization. A second-order upwind scheme is adopted for convective terms. Gradient terms are handled via a second-order cell-limited Gauss linear scheme. Crank-Nicolson is used as multistep integration schemes in the structural solver, and the timestep is set the same as that in the CFD solver for data transfer. The simulation time of each case is 15 wave periods to obtain stable results. A typical CPU time is about one hour per second in real time.

IV. RESULTS

In the simulation, the water free surface is initially still, and the membrane starts from a flat configuration. There are two phases of the motion response of the membrane. At phase one, the waves have not reached the device and the deformation of the membrane is driven by the hydrostatic pressure. After a while, the membrane reaches its equilibrium configuration and stops moving. At phase two, the membrane deforms periodically because of the waves that pass by.

A. Deformation under hydrostatic pressure

The flow field within the first transient phase is shown in Figure 4. It can be seen that the membrane deforms downwards from a flat state, holding the water weight above it. When it reaches its maximum deformation at approximately 0.1 s, it starts to bounce back to its highest tip location at 0.2 s. The oscillation continues almost periodically. This is due to the hydraulic and material damping effect. The free surface plot also reveals this feature, showing distinct convex or concave above the collector, which is caused by the change of fluid mass in the collector.

The time series of the tip displacement of the membrane is shown in Figure 5. The data marked blue is the time instants for t_1-t_6 in Figure 4. The amplitude of the oscillation decreases with time, with the maximum displacement of $|z_{tip}/r_c|=0.6$. When the motion becomes stable, the balance position of the tip is $|z_{tip}/r_c|=0.43$.

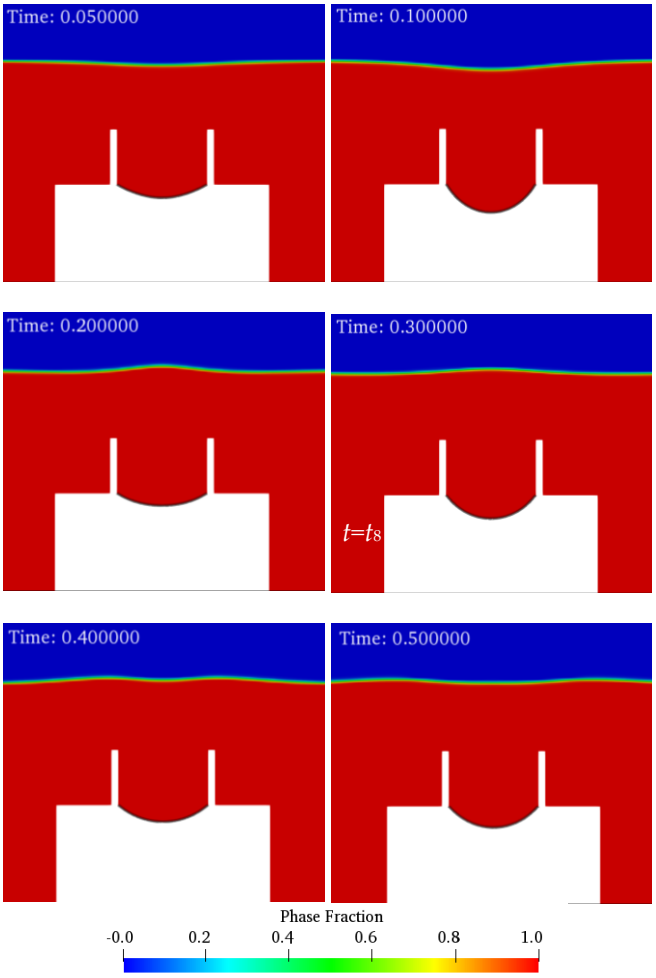

Figure 4 Free surface above the membrane from t_1=0.05s to t_6=0.5s. The blue and red areas represent air and water

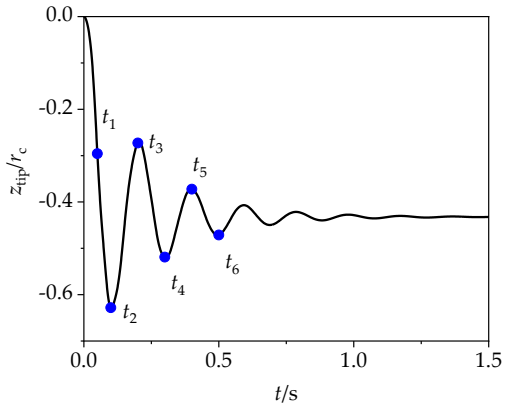

Figure 5 Tip displacement of the membrane within phase 1. The blue points correspond to t_1~t_6 in Figure 4.

B. *Deformation under hydrodynamic pressure*

The profile during deformation of the membrane with waves propagating is shown in Figure 6, where the wave period and wave height are 1.4 s and 0.1 m, respectively. The grey line in this figure represents the membrane profile at its maximum deformation. The wave direction points to the right. It can be seen that the wave crest reaches the device at t_8 at which the deformation reaches its maximum. As the wave propagates, when the wave trough arrives at t_{11} the membrane bounces back reaching to its minimum deformation. Referring to the calculated velocity field, it can be found that a vortex forms in the collector, which is generated at the instants in which the wave crest reaches the device. It circles around the centre of the collector, with a speed of almost zero in the centre. The high speed at the edge of the vortex does close to the membrane, which influences the motion response of membrane.

The tension along the membrane at different time,shown in Figure 7, reveals that the tension force is nearly uniformly distributed along the membrane. This feature is beneficial to the durability of such WEC device. In addition, the tension rises with an increasing deformation, which has a maximum pressure of 7.2*10^5 Pa.

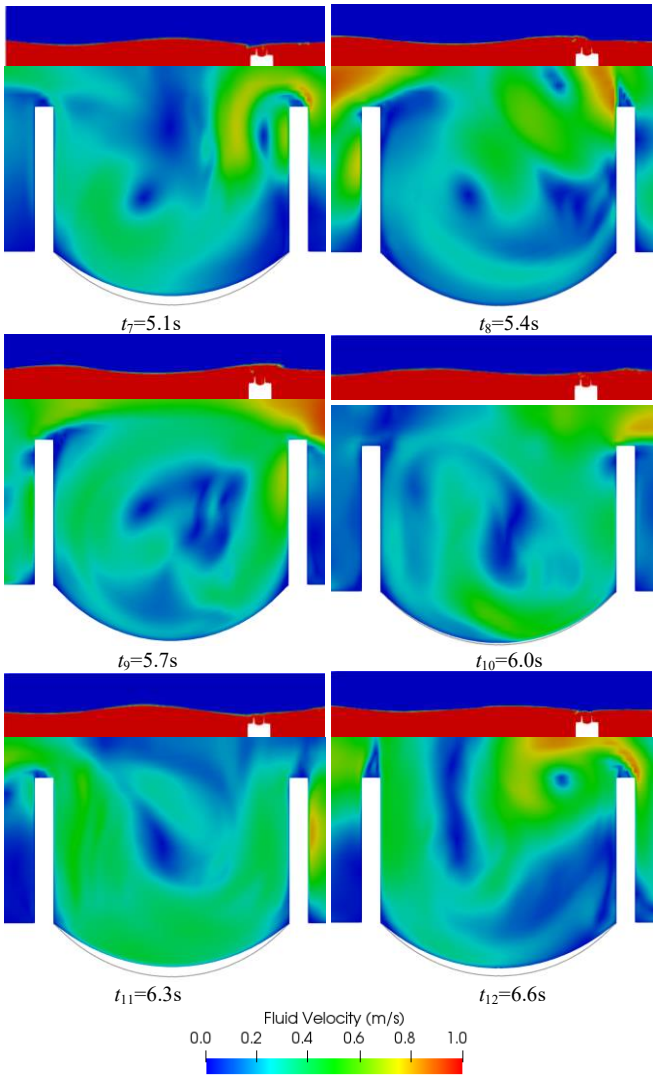

Figure 6 Free surface in the wave tank and velocity field around the collector from t_7=5.1s to t_{12}=6.6s. upper image is the volume fraction field in the whole tank. The lower image is the zoomed-in velocity field around the collector. The solid curve below the membrane is the maximum deformation position for comparison.

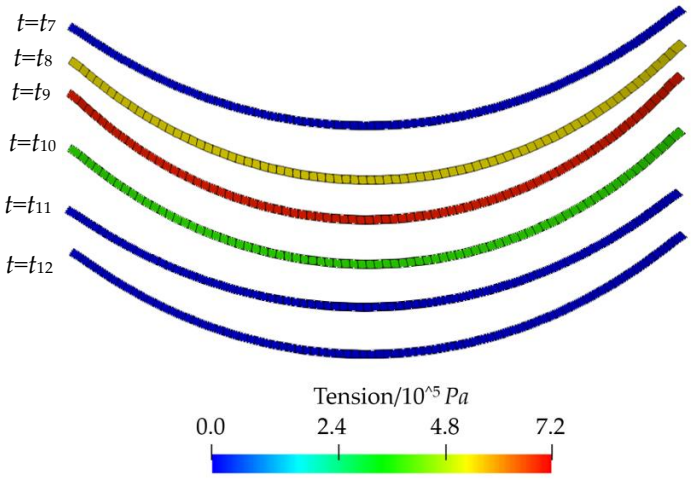

Figure 7 Shape and tension of the membrane from t_7=5.1s to t_{12}=6.6

In this study, the dynamic response of a flexible WEC without a collector is also tested to investigate collector effect on the membrane. Figure 8 shows the velocity field around the membrane without a collector. Compared to the case with collector in Figure 6, the absence of the collector leads to a significant difference. In particular, the velocity distributes more uniformly without vortex generation, and the velocity near the membrane is low. As a results of fluid field change, the deformation of membrance is varied as shown in Figure 89.

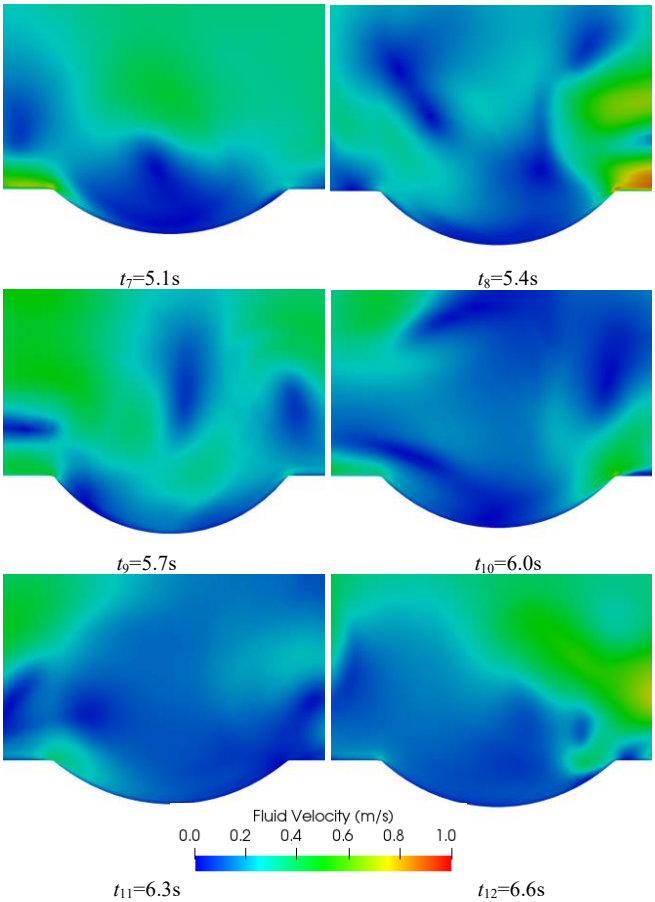

Figure 8 Velocity field around the collector from t_7=5.1s to t_{12}=6.6s

As seen,with the collector, the flow field becomes more irregular, leading to some small fluctuations onto tip displacement curve. The 'influenced zone' of the high velocity field is larger and closer to the membrane with a collector, which further induces a larger deformation. The fluctuations are mainly induced by the complex turbulent flow inside collector.

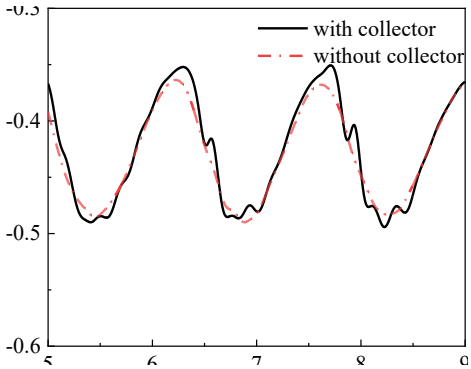

Figure 9 Tip displacement for a flexible WEC

C. *Deformation under different wave periods*

Traditional WEC, such as point absorber or oscillating water column, usually works favourably for a specific wave period. The efficiency of device decreases significantly, even does not produce any energy, if the sea state is too far from the design condition. The performance under different wave periods of this flexible structure WEC is investigated. The displacement of membrane is shown in Figure 10 together with the data from experiment. To compare the deformation degree associated with different cases, which have different mean tip displacement, the deformation is represented by the maximum/minimum tip displacement subtracted by its means tip displacement. Because the constitutive law of the material in the present CFD work is different from that in the experiment, the experimental and the simulation results are not directly comparable. However, similar trend for displacement vs frequency are presented, i.e., the peak deformation occurs between T=1.4 s-1.6 s, which has also been observed in experiments. It is attributed to an effect of the dynamic resonant response of the system, which is well captured by the CFD model

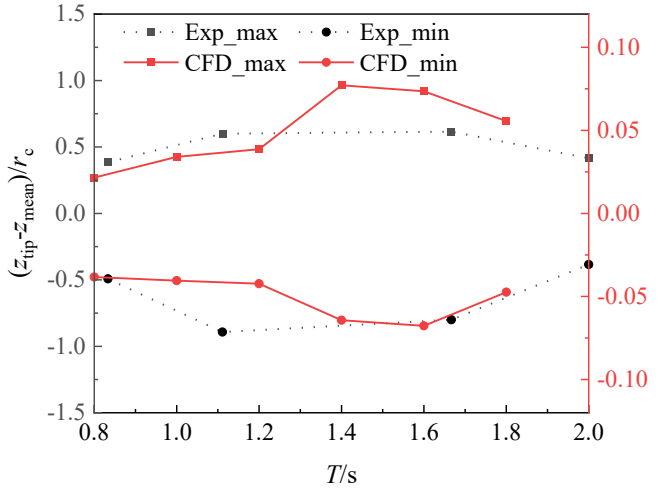

Figure 10 Maximum and minimum tip displacement with T=0.8 s-2.0 s. Red lines is the maximum and minimum tip displacement of CFD results and black dashed lines is that of the experimental results

V. CONCLUSION

The present work aims at studying an FSI problem of a novel flexible structure WEC based on dielectric elastomers. A coupled CFD-MBD tool is developed, with the dynamic response of a flexible membrane under regular waves being numerically simulated. For the sake of simpliciation, the membrane is modelled as an equivalent two-dimensional beam. The CFD results reveal some qualititave trends of experimental testing under different regular wave conditions. Moreover, we found that the existance of the collector increases the turbulence of fluid flow, leading to a larger deformation of membrane. Although a peak period corresponding to a maximum deformation exists, the deformation is not very sensitive to the wave frequency. This indicates that such flexible WEC has a strong adaptability to the variation of sea states, rather than preferring a very specific wave parameter. Future work will focus on developing nonlinear hyper-elastic model for the dielectric elastomer membrane using three-dimensional modelling, which is able to describe large deformation, similar to the real device response.

ACKNOWLEDGEMENT

REFERENCES

[1] Henderson, R., 2006. Design, simulation, and testing of a novel hydraulic power take-off system for the Pelamis wave energy converter. Renewable energy, 31(2), pp.271-283.

[2] Cameron, L., Doherty, R., Henry, A., Doherty, K., Van't Hoff, J., Kaye, D., Naylor, D., Bourdier, S. and Whittaker, T., 2010, October. Design of the next generation of the Oyster wave energy converter. In 3rd international conference on ocean energy (Vol. 6, p. 1e12).

[3] Moretti, G., Herran, M.S., Forehand, D., Alves, M., Jeffrey, H., Vertechy, R. and Fontana, M., 2020. Advances in the development of dielectric elastomer generators for wave energy conversion. Renewable and Sustainable Energy Reviews, 117, p.109430.

[4] Moretti, G., Papini, G.P.R., Righi, M., Forehand, D., Ingram, D., Vertechy, R. and Fontana, M., 2018. Resonant wave energy harvester based on dielectric elastomer generator. Smart Materials and Structures, 27(3), p.035015.

[5] Moretti, G., Fontana, M. and Vertechy, R., 2015. Model-based design and optimization of a dielectric elastomer power take-off for oscillating wave surge energy converters. Meccanica, 50(11), pp.2797-2813.

[6] Michailides, C. and Angelides, D.C., 2015. Optimization of a flexible floating structure for wave energy production and protection effectiveness. Engineering Structures, 85, pp.249-263.

[7] Zhang, X., Lu, D., Guo, F., Gao, Y. and Sun, Y., 2018. The maximum wave energy conversion by two interconnected floaters: Effects of structural flexibility. Applied Ocean Research, 71, pp.34-47.

[8] Babarit, A., Singh, J., Mélis, C., Wattez, A. and Jean, P., 2017. A linear numerical model for analysing the hydroelastic response of a flexible electroactive wave energy converter. Journal of Fluids and Structures, 74, pp.356-384.

[9] Kurniawan, A., Chaplin, J.R., Greaves, D.M. and Hann, M., 2017. Wave energy absorption by a floating air bag. Journal of Fluid Mechanics, 812, pp.294-320.

[10] E. Renzi, "Hydroelectromechanical modelling of a piezoelectric wave energy converter," *Proceedings of the Royal Society A: Mathematical, Physical and Engineering Sciences,* vol. 472, no. 2195, p. 20160715, 2016

[11] S. Zheng, D. Greaves, M. H. Meylan, and G. Iglesias, "Wave power extraction by a submerged piezoelectric plate," in *Developments in Renewable Energies Offshore: Proceedings of the 4th International Conference on Renewable Energies Offshore (RENEW 2020, 12-15 October 2020, Lisbon, Portugal)*, 2020: CRC Press, p. 149.

[12] Liu, Y., Xiao, Q., Incecik, A. and Peyrard, C., 2019. Aeroelastic analysis of a floating offshore wind turbine in platform-induced surge motion using a fully coupled CFD-MBD method. Wind Energy, 22(1), pp.1-20.

[13] OpenFOAM, 2018, "The OpenFOAM Foundation Website."

[14] MBDyn, 2018, "Homepage of Free MultiBody Dynamics Simulation MBDyn."

[15] Zhou, Y., Xiao, Q., Liu, Y., Incecik, A., Peyrard, C., Li, S. and Pan, G., 2019. Numerical modelling of dynamic responses of a floating offshore wind turbine subject to focused waves. Energies, 12(18), p.3482.

[16] Righi, M., Moretti, G., Forehand, D., Vertechy, R., Fontana, M., 2021, A broadbanded pressure differential wave energy converter based on dielectric elastomer generators. Nonlinear Dynamics (under review).